Data Repository Item

Appendix DR1

(U-Th)/He sample preparation and analytical techniques

Apatite separates for (U-Th)/He analyses were produced from eastern Tibet granitoids collected during field campaigns in 1998 and 2001 (Table DR1). Grains were initially selected for euhedral morphology and scanned for visible inclusions of potentially high U or Th- rich phases under a ~120 power binocular microscope using cross-polars. Prior to analysis, grains were measured for the alpha-ejection correction (*Farley et al., 1996; Farley, 2000*). For multi-grain aliquots, a mass-weighted average grain radius was determined for the alpha-ejection correction.

Helium outgassing was performed by both furnace heating and laser heating procedures (*House et al., 1999; House et al., 2000*). Furnace samples are denoted as such in Table DR2. Additional single-grain laser replicate analyses were performed on a subset of the furnace samples in order to demonstrate consistency between the two techniques used for this survey. While lithology of a particular sample played the primary role in grainsize and quality of available grains, the lower blanks, and the single-grain analyses afforded by laser analysis resulted in overall lower analytical uncertainties, smaller F_t corrections, and a higher number of replicate analyses. We limited our dataset to include grains of radii 34 – 80 µm, resulting in typical alpha-ejection corrections of 18-35% (F_t = 0.65 - 0.83; Table DR2).

After outgassing, grains were retrieved, dissolved and spiked with ^{235}U and ^{230}Th and analyzed in a Finnigan Element inductively couple plasma mass spectrometer (ICPMS). Anomalously high ratios of Th/U possibly indicate the presence of Th rich phases (such as monazite) (*House et al., 2001*) and these analyses were excluded. Low He yields (near blank level) are susceptible to implantation from surrounding phases, and are also excluded from our final results. The number of replicate analyses varied with the amount and quality of sample material. Some samples simply did not yield sufficient quality material for more than one replicate analysis.

Mean ages are reported only for samples with more than one replicate (Table DR3). Propagated errors on He ages based on the analytical uncertainty in U, Th, and He measurements are 4% (2-sigma) for laser samples and 6% (2-sigma) for furnace samples (*Farley, 2002*), however we report a 6% (2-sigma) uncertainty for all samples based on the reproducibility of laboratory standards (*Farley, 2002*). Mean errors are reported at 1-sigma as standard errors using the standard deviation of the replicate analyses divided by (n-1) where n is the number of replicate analyses performed (Table DR3). This error estimate is larger than the analytical error alone and is intended to reflect the age uncertainty due to differences in grain size, minor crystal defects, zoning of parent material and other factors which may contribute to grain to grain differences in He age and uncertainties in the alpha-ejection correction [i.e. (*House et al., 2001*)].

In general, age variability is greater for single-grain replicate analyses compared to multigrain replicate aliquots that average several to tens of grains. Several ages from the Daocheng transect have large absolute uncertainties but have similar relative uncertainties when compared to younger samples.

Apatite fission-track sample preparation and analytical techniques

AFT analyses were performed by Raymond A. Donelick at Apatite to Zircon, Inc., Viola, Idaho, U.S.A. following the procedures and methods outlined in (*Burtner et al., 1994*) and the 252Cf irradiation procedure described by (*Donelick and Miller, 1991*). The only significant change in sample preparation since 1994 is that samples are irradiated in position D-9 for 45 minutes at the Washington State University Nuclear Radiation Center 1 MW TRIGA nuclear reactor. The parameter Dpar (Table DR4) is described in detail by (*Carlson et al., 1999*).

Depth datum calculation and depth/age relationships

Comparison of ages along our individual transects require that we consider our samples relative to a common surface datum beneath which the samples would have cooled. Exhumation rate and the timing of exhumation rate change are most accurately determined when samples are plotted relative to a datum beneath which the low-temperature isotherms are horizontal. Shallow isotherms in the crust mimic the topographic surface at wavelengths generally greater than a few tens of kilometers depending on the amplitude of the topography and the erosion rate (*Stüwe et al., 1994*). We expect shallow isotherms to lie parallel to the long-wavelength, gentle slope of the southeastern plateau surface which is defined by the regional low-relief relict landscape (*Clark, 2003*). The regional continuity and long-wavelength nature of this surface makes it a sensible datum beneath which to consider data from different geographic localities.

The depth of each sample transect beneath the regional, relict landscape can be determined by subtracting each sample elevation from the average elevation of the nearest surface remnant. This yields a minimum estimate of sample depth because it assumes that no erosion of the surface has occurred since initiation of rapid river incision. In most cases this depth estimation is sensitive to the local relief observed across the surface (<600 m), resulting in an average depth uncertainty of ±300 m for each transect relative to each other. The exception is for the Dadu and Anning transects where a rare vertical offset of the relict landscape of ~ 1 km occurs across the Xianshuihe Fault. Therefore the depth determination of this transect has greater uncertainty associated with it, than with other sample transects where samples can be tied to a single elevation datum (i.e. tied to a single surface elevation with the uncertainty associated with the local relief described above).

Where abrupt changes in the depth/age gradient are observed, as it is when we consider our data on a regional basis, the timing of such change can be used to constrain the initiation of rapid exhumation. While the position of the change in age/depth gradient is not well defined by our dataset, the ~ 1 km depth interval of rapidly cooled samples of the the Danba and Yalong transects best define the timing of rapid river incision.

The depth/age relationships are consistent for both the Danba and Yalong transects with two exceptions. First, the lowest most sample on the Yalong transect (sample 01-26 (*Table DR1-DR4*), is anomalously old compared to the other samples at slightly higher elevations. Because this sample was collected only a few hundred meters from sample 01-25 and a few kilometers from 01-27, and because the apatite fission-track age on this sample does not show the same depth/age relationship with other nearby samples, variations in geothermal gradient, lithology, or spatial variability in erosion rate are likely not to be the cause of the anomalous (U-Th)/He age. Furthermore, the pooled AFT age on sample 01-26 is younger than the mean (U-Th)/He age, which we do not observe on any of our other samples. We suggest that the anomalous (U-Th)/He age for 01-26 most likely reflects local processes occurring near this sample rather than regional conductive cooling. Second, the depth/age gradient of the Yalong AFT data is negative. However, considered with the Danba AFT data, these data still crudely define a positive depth/age gradient with scatter that is consistent with the (U-Th)/He data. All three samples are within error of the (U-Th)/He data, and samples 01-25 and 01-27 have pooled ages that are greater than the mean (U-Th)/He ages, also suggesting consistency between the two thermochronometers with the exception of the anomalous 01-26 sample discussed above.

Thermal Modeling

We use a standard finite-difference algorithm to solve the partial differential equation governing heat conduction-advection:

$$\frac{\partial T}{\partial t} = \kappa\left(\frac{\partial^2 T}{\partial z^2}\right) + u(t)\left(\frac{\partial T}{\partial z}\right) + \frac{A}{K}$$

where T is temperature, κ is the thermal diffusivity, u is the material velocity with respect to the surface (e.g. erosion rate), A is the heat production per unit volume per unit time, and K is the thermal conductivity. For reasonable values of crustal heat production, the effect of including the production term (A/K) is small, therefore for simplicity we set this term to zero (e.g. *Moore and England*, 2001). We used a constant surface temperature of 10 °C, a uniform thermal diffusivity of 10^6 $m^2 \cdot s^{-1}$, and a nodal spacing of 0.1 km. The initial geotherm was assumed to be linear, and the lower boundary at the base of the lithosphere was maintained at 100 km depth. (Note that the temperature structure below ~20 km depth will not significantly affect results over the time scales considered here.) The time-temperature history is computed by allowing the upper surface (held at constant temperature) to move downward through the grid at a rate equal to the erosion rate (u).

(U-Th)/He ages were computed from a second finite-difference algorithm that calculates age as a function of the thermal history of the sample for an average grain radius of 54.29 μm and a nodal spacing of 0.21 μm (*Wolf et al*., 1998; *Farley*, 2000). AFT cooling ages were determined by using a range of nominal closure temperatures between 90–110 °C (e.g., *Green et al.*, 1986, and references therein).

References

Burchfiel, B.C., Chen, Z., Liu, Y., and Royden, L.H., 1995, Tectonics of the Longmen Shan and adjacent regions, Central China: International Geology Review, v. 37, p. 661–735.

Burtner, R. L., Nigrini, A., and Donelick, R. A., 1994, Thermocrhonology of Lower Cretaceous source rocks in the Idaho-Wyoming thrust belt: American Association of Petroleum Geologists Bulletin, v. 78, n. 10, p. 1613 – 1636.

Carlson, W. D., Donelick, R. A., and Ketcham, R. A., 1999, Variability of apatite fission track annealing kinetics I: Experimental results: American Mineralogist, v. 84, p. 1213 – 1223.

Clark, M.K., 2003, Late Cenozoic uplift of southeastern Tibet [Ph.D. thesis]: Cambridge, Massachusetts, Massachusetts Institute of Technology, 236 p.

Donelick, R. A. and Miller, D. S., 1991, Enhanced TINT fission track densities in low spontaneous track density apatites using 252Cf-derived fission track fragment tracks: A model and experimental observations: Nuclear Tracks and Radiation Measurements, v. 18, p. 301 – 307.

Farley, K. A., Wolf, R. W., Silver, L. T., 1996, The effects of long-stopping distances on (U-Th)/He ages, Geochim. Cosmochim. Acta, v. 60, p. 4223 - 4229.

Farley, K. A., 2000, Helium diffusion from apatite; general behavior as illustrated by Durango fluorapatite: Journal of Geophysical Research, v. 105, p. 2903-2914.

Farley, K. A., 2002, (U-Th)/He Dating: Techniques, Calibrations, and Applications, Noble gases in geochemistry and cosmochemistry: Reviews in Mineralogy and Geochemistry, v. 47, p. 819-843.

Green, P.F., Duddy, I.R., Gleadow, A.J.W., Tingate, P.R., and Laslett, G.S., 1986, Thermal annealing of fission tracks in apatite, 1. A qualitative description: Chemical Geology, v. 59, p. 237–253.

House, M. A., Farley, K. A., and Kohn, B. P., 1999, An empirical test of helium diffusion in apatite: borehole data from the Otway basin, Australia: Earth and Planetary Science Letters, v. 170, p. 463-474.

House, M. A., Farley, K. A., and Stockli, D., 2000, Helium chronometry of apatite and titanite using Nd-YAG laser heating: Earth and Planetary Science Letters, v.183, n. 3-4, p. 365-368.

House, M. A., Wernicke, B. P., and Farley, K. A., 2001, Paleo-geomorphology of the Sierra Nevada, California, from (U-Th)/He ages in apatite: American Journal of Science, v. 301, p. 77-102.

Moore, M.A., and England, P.C., 2001, On the inference of denudation rates from cooling ages minerals: Earth and Planetary Science Letters, v. 185, p. 265–284.

Stüwe, K., White, L., and Brown, R., 1994, The influence of eroding topography on steady-state isotherms. Application to fission track analysis: Earth and Planetary Science Letters, v. 124, p. 63 – 74.

Wang, E., Burchfiel, B.C., Royden, L.H., Chen, L., Chen, J., Li, W., and Chen, Z., 1998, Late Cenozoic Xianshuihe-Xiaojiang, Red River, and Dali fault systems of southwestern Sichuan and central Yunnan, China: Geological Society of America Special Paper, v. 327, 108 p.

Wolf, R.A., Farley, K.A., and Kass, D.M., 1998, Modeling of the temperature sensitivity of the apatite (U-Th)/He thermochronometer: Chemical Geology, v. 148, n. 1–2, p. 105-114.

TABLE DR1. SAMPLE DESCRIPTIONS

Transect	Sample ID	Rock Type	Age (Ma)	Lon (°N)	Lat (°E)	Elev (m)	Depth* (m)
Anning	98-17	granodiorite	Mz	102.0933	28.1985	1650	2150
	98-18	granite	Pt	102.1322	27.7119	1750	2050
	98-19	granite	Pt	102.0964	27.7059	2200	1600
	98-20	granite	Pt	102.0856	27.6999	2300	1500
Dadu	98-9	granite	Pt	102.3871	29.1724	1050	1950
	98-10	granite	Pt	102.3602	29.1474	1150	1850
	98-11	granite	Pt	102.3408	29.1282	1200	1800
	98-12	granite	Pt	102.3396	29.0886	1450	1550
Danba	01-11	granite	Mz	101.9297	31.1980	2840	1960
	01-12	granite	Mz	101.9262	31.1951	2580	2220
	01-13	granite	Mz	101.9241	31.1937	2500	2300
	01-14	granite	Mz	101.9290	31.2042	3000	1800
	01-15	granite	Mz	101.9320	31.1733	2100	2700
Daocheng	01-37	granite	Mz	100.3529	29.6446	3860	840
	01-38	granite	Mz	100.3447	29.6346	3980	720
	01-39	granite	Mz	100.3385	29.6218	4100	600
	01-40	granite	Mz	100.3165	29.5741	4200	500
	01-41	granite	Mz	100.2764	29.5322	4500	200
	01-42	granite	Mz	100.2695	29.5162	4640	60
	01-43	granite	Mz	100.1955	29.4605	4620	80
	01-44	granite	Mz	100.1261	29.3575	4420	280
	01-48	granite	Mz	100.0878	29.2360	4020	680
Pamai	01-49	granite	Mz	101.5319	30.1241	4000	300
Yalong	01-25	granodiorite	Mz	101.7510	28.5425	1700	2800
	01-26	granite	Mz	101.7480	28.5342	1620	2880
	01-27	granite	Mz	101.7335	28.5520	1950	2550
	01-28	granite	Mz	101.6400	28.6533	2100	2400
	01-29	granite	Mz	101.6034	28.8347	2550	1950
	01-30	granite	Mz	101.5734	28.8742	2750	1750

*Measured from local remnant surface elevation, positive downward. This measurement is a minimum estimate of the position of each sample beneath the Earth's surface when rapid river incision commenced.

TABLE DR2. (U-TH)/HE REPLICATE ANALYSES

Transect	Sample Replicate	[U] (ppm)	[Th] (ppm)	U/Th	[^{4}He] (nmol/g)	Radius (μm)	Length (μm)	FT	Raw Age (Ma)	Corr Age* (Ma)	Error† 2σ
Anning	MC9817LC	4.5	3.7	1.22	0.229	56	194	0.77	7.9	10.3	0.6
Anning	MC9817LD	5.3	3.0	1.76	0.632	70	285	0.82	19.3	23.7	1.4
Anning	MC9818[f]	10.8	24.3	0.44	0.955	34	200	0.66	10.7	16.1	1.0
Anning	Mc9818LA	15.6	28.1	0.55	2.199	77	251	0.83	18.2	21.9	1.3
Anning	MC9818LC	20.8	29.7	0.70	2.390	57	223	0.78	16.0	20.0	1.2
Anning	MC9819[f]	12.4	9.4	1.32	1.198	45	181	0.73	15.0	20.7	1.2
Anning	MC9819LA	10.0	4.7	2.10	0.790	53	246	0.77	13.1	17.1	1.0
Anning	MC9819LB	15.6	15.8	0.99	1.231	40	200	0.70	11.7	16.7	1.0
Anning	MC9820[f]	9.0	17.3	0.52	1.127	36	135	0.65	15.9	24.3	1.5
Dadu	MC9809[f]	10.4	52.0	0.42	0.687	38	143	0.67	5.6	8.3	0.5
Dadu	MC9809BMH	3.6	16.3	0.22	0.057	60	180	0.74	1.4	1.9	0.1
Dadu	MC9810A[f]	9.8	50.6	0.19	1.914	40	149	0.69	16.2	23.5	1.4
Dadu	MC9810C[f]	6.1	34.4	0.18	0.539	35	163	0.66	7.0	10.6	0.6
Dadu	MC9811[f]	6.0	25.3	0.23	0.761	45	174	0.72	11.8	16.4	1.0
Dadu	MC9811B[f]	5.3	18.3	0.29	0.687	35	168	0.67	13.2	19.9	1.2
Dadu	mc9812aa	6.2	35.7	0.17	1.798	69	189	0.77	22.7	29.5	1.8
Dadu	MC9812BMH	16.6	59.7	0.28	1.678	74	283	0.80	10.1	12.6	0.8
Dadu	mc9812cc	3.6	16.6	0.22	0.655	63	240	0.77	16.1	21.0	1.3
Danba	MC0111A	30.1	17.2	1.76	1.336	54	189	0.74	7.2	9.7	0.6
Danba	MC0111B	27.3	16.2	1.69	0.839	63	266	0.78	5.0	6.3	0.4
Danba	MC0111D	27.6	15.4	1.79	1.005	46	266	0.72	5.9	8.2	0.5
Danba	MC0112A	242.6	164.4	1.48	6.362	43	274	0.70	4.2	5.9	0.4
Danba	MC0112B	105.3	63.9	1.65	2.687	49	154	0.71	4.1	5.8	0.4
Danba	MC0112C	53.9	24.5	2.20	1.898	63	326	0.79	5.6	7.4	0.5
Danba	MC0112D	77.9	115.6	0.67	2.082	49	154	0.70	3.7	5.2	0.3
Danba	MC0113A	167.8	81.4	2.06	4.554	69	309	0.80	4.5	5.6	0.3
Danba	MC0113B	97.0	49.8	1.95	2.717	63	300	0.79	4.6	5.9	0.4
Danba	MC0113C	97.3	44.4	2.19	2.406	46	163	0.70	4.1	5.9	0.4
Danba	MC0113D	129.2	72.1	1.79	3.093	49	326	0.74	3.9	5.3	0.3
Danba	MC0114B	20.5	21.6	0.95	1.704	51	171	0.72	12.2	16.9	1.0
Danba	MC0114C	16.5	19.6	0.84	0.737	51	206	0.73	6.4	8.8	0.5
Danba	MC0114D	28.1	32.0	0.88	1.131	63	231	0.77	5.8	7.5	0.5

Transect	Sample Replicate	[U] (ppm)	[Th] (ppm)	U/Th	[^{4}He] (nmol/g)	Radius (μm)	Length (μm)	FT	Raw Age (Ma)	Corr Age* (Ma)	Error† 2σ
Danba	MC0114E	36.2	40.8	0.89	1.377	51	189	0.73	5.5	7.6	0.5
Danba	MC0114F	18.6	17.8	1.04	0.724	51	180	0.73	5.9	8.1	0.5
Danba	MC0114G	12.9	10.3	1.25	0.430	54	137	0.72	5.2	7.2	0.4
Danba	MC0115A	201.8	162.2	1.24	4.641	54	223	0.75	3.6	4.8	0.3
Danba	MC0115B	60.7	25.3	2.40	1.567	63	223	0.78	4.3	5.6	0.3
Danba	MC0115C	81.2	36.9	2.20	2.075	57	334	0.77	4.3	5.5	0.3
Danba	MC0115D	70.0	33.4	2.10	1.939	49	283	0.74	4.6	6.2	0.4
Danba	MC0115E	139.3	78.0	1.83	3.453	51	274	0.75	4.0	5.4	0.3
Daocheng	MC0137B	9.3	13.9	0.67	2.655	63	223	0.77	38.9	50.4	3.0
Daocheng	MC0137C	6.0	11.2	0.54	1.659	49	137	0.69	35.1	50.6	3.0
Daocheng	MC0137D	7.9	13.2	0.60	2.260	74	129	0.77	37.6	49.1	3.0
Daocheng	MC0138a	46.5	49.4	0.94	8.296	43	160	0.68	26.2	38.6	2.3
Daocheng	MC0138c	27.6	82.7	0.33	12.702	43	120	0.65	49.5	75.9	4.6
Daocheng	MC0138d	9.7	23.0	0.42	3.709	46	154	0.69	45.1	65.8	4.0
Daocheng	MC0139c	11.6	30.1	0.38	4.817	51	206	0.73	47.4	65.4	3.9
Daocheng	MC0140A	14.6	23.1	0.63	10.285	40	231	0.68	93.6	138.7	8.3
Daocheng	MC0140C	11.9	33.4	0.36	7.571	51	257	0.73	70.1	95.6	5.7
Daocheng	MC0140E	16.0	49.3	0.32	11.246	51	223	0.73	74.6	102.5	6.2
Daocheng	MC0141a	24.5	68.8	0.36	23.716	54	206	0.74	106.5	144.7	8.7
Daocheng	MC0141c	25.2	62.2	0.41	16.278	51	154	0.71	74.8	105.2	6.3
Daocheng	MC0141d	25.3	68.9	0.37	13.178	46	137	0.68	58.1	85.8	5.2
Daocheng	MC0142A	8.6	16.0	0.53	5.327	74	206	0.79	79.0	99.7	6.0
Daocheng	MC0142B	11.9	27.2	0.44	10.830	57	189	0.74	108.2	145.6	8.7
Daocheng	MC0142C	40.0	93.7	0.43	12.201	69	229	0.78	36.1	46.1	2.8
Daocheng	MC0142D	12.6	23.3	0.54	5.754	57	206	0.75	58.3	77.8	4.7
Daocheng	MC0143A	11.3	24.4	0.46	6.127	54	206	0.74	65.8	89.2	5.4
Daocheng	MC0143B	14.5	40.1	0.36	8.487	46	189	0.70	65.1	93.6	5.6
Daocheng	MC0144A	24.2	50.2	0.48	18.179	49	214	0.72	92.8	128.9	7.7
Daocheng	MC0144B	17.4	87.0	0.20	11.202	54	197	0.73	54.3	74.5	4.8
Daocheng	MC0148A	62.3	71.5	0.87	20.935	46	189	0.70	48.5	69.1	4.1
Pamai	MC0149a	34.3	39.0	0.88	9.908	60	266	0.77	41.8	54.2	3.3
Pamai	MC0149b	31.9	54.4	0.59	12.924	63	206	0.77	53.0	69.2	4.1
Pamai	MC0149c	26.7	28.8	0.93	7.227	54	240	0.75	39.6	52.9	3.2
Pamai	MC0149e	23.8	27.4	0.87	7.365	57	274	0.76	44.7	58.5	3.5

Transect	Sample Replicate	[U] (ppm)	[Th] (ppm)	U/Th	[^{4}He] (nmol/g)	Radius (μm)	Length (μm)	FT	Raw Age (Ma)	Corr Age* (Ma)	Error[†] 2σ
Pamai	MC0149f	17.8	42.8	0.41	6.438	54	206	0.74	42.4	57.6	3.5
Pamai	MC0149g	44.4	58.4	0.76	13.006	63	214	0.77	41.0	53.3	3.2
Yalong	MC0125A	5.3	2.1	2.49	0.085	74	214	0.80	2.7	3.4	0.2
Yalong	MC0125B	27.8	6.7	4.17	0.671	57	189	0.75	4.2	5.6	0.3
Yalong	MC0125D	19.6	17.2	1.14	0.467	56	257	0.76	3.6	4.8	0.3
Yalong	MC0126A	10.8	18.4	0.59	0.600	57	171	0.74	7.3	9.9	0.6
Yalong	MC0126B	25.0	146.0	0.17	2.355	80	291	0.81	7.3	9.0	0.5
Yalong	MC0126D	11.5	17.0	0.68	0.831	57	154	0.74	9.9	13.4	0.8
Yalong	MC0127A	17.2	21.6	0.80	0.361	54	274	0.75	3.0	4.0	0.2
Yalong	MC0127B	8.1	6.3	1.29	0.167	63	206	0.77	3.2	4.1	0.3
Yalong	MC0127D	17.7	17.1	1.03	0.627	57	274	0.76	5.3	7.0	0.4
Yalong	MC0128A	14.4	4.8	2.98	0.191	46	223	0.71	2.3	3.2	0.2
Yalong	MC0129cc	17.4	2.0	8.83	0.737	57	180	0.75	7.6	10.1	0.6
Yalong	MC0129dd	9.2	1.4	6.79	0.319	57	180	0.75	6.2	8.2	0.5
Yalong	MC0129ee	12.5	2.3	5.53	0.602	46	189	0.71	8.5	12.0	0.7
Yalong	MC0129ff	14.4	3.0	4.82	0.310	46	291	0.72	3.8	5.2	0.3
Yalong	MC0129gg	35.3	1.6	22.63	0.873	46	326	0.73	4.5	6.2	0.4
Yalong	MC0130A	3.3	5.5	0.60	0.234	63	171	0.76	9.5	12.5	0.8
Yalong	MC0130B	11.2	30.4	0.37	0.174	49	206	0.71	1.7	2.4	0.2
Yalong	MC01-30A	8.0	19.9	0.40	1.063	63	309	0.78	15.5	19.9	1.2
Yalong	MC0130cc	3.6	3.8	0.96	0.099	57	197	0.75	4.0	5.4	0.3

[f]Furnace sample

*Corrected for alpha-ejection after *Farley et al*. (1996).

[†]Errors on single replicate analyses are 6 percent (2σ) and represent uncertainty on reproducibility of laboratory standards (*Farley*, 2002).

TABLE DR3: (U-TH)/HE MEAN AGES

Transect	Sample ID	No. Replicates (n)	Mean Age* (Ma)	Std Error[†] (1σ)
Anning	98-17	2	17.0	6.7
	98-18	3	19.5	2.1
	98-19	3	18.2	1.5
Dadu	98-9	2	5.1	3.2
	98-10	2	17.0	6.5
	98-11	2	18.1	1.8
	98-12	3	21.0	6.0
Danba	01-11	3	8.1	1.2
	01-12	4	6.1	0.5
	01-13	4	5.7	0.1
	01-14	6	9.4	1.7
	01-15	5	5.5	0.3
Daocheng	01-37	3	50.0	0.6
	01-38	3	60.1	11.1
	01-40	3	112.3	16.4
	01-41	3	111.9	21.2
	01-42	4	92.3	24.1
	01-43	2	91.4	2.2
	01-44	2	101.7	27.2
Pamai	01-49	6	57.6	2.7
Yalong	01-25	3	4.6	0.8
	01-26	3	10.8	1.6
	01-27	3	5.0	1.2
	01-29	5	8.3	1.4
	01-30	4	10.1	4.5

*4 individual samples yielded only one replicate analysis and are not included with the mean ages. See Table DR2.

[†]The standard error (std error) was computed from replicate analyses for each sample individually (std. deviation of replicates/$\sqrt{(n-1)}$). In the case where only 2 replicates were analyzed, the error is reported as half of the age difference.

TABLE DR4: APATITE FISSION-TRACK AGES

Transect	Sample	ρ_s*	ρ_i*	ρ_d*	Grains (dmnls)	Q (dmnls)	Dpar (μm)	Dper (μm)	Mean Length (μm)	Std Dev (μm)	Pooled FT Age[†] (Ma)
Danba	01-11	0.179 (106)	4.841 (2863)	4.004 (4115)	21	0.487	1.74	0.48	13.55 ± 0.32 (111)	1.64	8.43 ± 0.87 [1.74]
	01-12	0.641 (272)	14.52 (6161)	4.002 (4115)	24	0.395	1.90	0.44	13.63 ± 0.30 (114)	1.64	10.00 ± 0.70 [1.40]
	01-13	0.764 (303)	16.731 (6639)	4.006 (4115)	18	0.234	1.97	0.45	13.44 ± 0.40 (110)	2.07	10.40 ± 0.70 [1.40]
	01-14	0.153 (96)	3.311 (2083)	4.007 (4115)	21	0.353	1.82	0.40	13.67± 0.36 (100)	1.82	10.50 ± 1.10 [2.20]
	01-15	0.957 (470)	24.574 (12063)	4.003 (4115)	22	0.026	2.01	0.45	13.96 ± 0.34 (110)	1.74	8.87 ± 0.49 [0.98]
Yalong	01-25	0.064 (34)	2.598 (1372)	3.997 (4115)	22	0.769	1.77	0.47	13.93 ± 0.46 (53)	1.68	5.63 ± 0.99 [1.98]
	01-26	0.058 (35)	2.068 (1247)	3.999 (4115)	23	0.618	1.66	0.42	13.71 ± 0.60 (32)	1.69	6.38 ± 1.11 [2.22]
	01-27	0.042 (35)	2.023 (1682)	4.000 (4115)	24	0.488	1.63	0.43	13.47 ± 1.02 (13)	1.76	4.73 ± 1.32 [1.64]

Note: Number of tracks counted or measured is shown in parentheses.

*Track densities are 10^6 tracks cm^{-2}. Abbreviations used are: ρ_s = spontaneous track densities; ρ_i = induced track densities; ρ_d = induced track densities in mica detector over standard glass.

[†]Uncertainties are quoted at 1σ and 2σ [in square brackets].

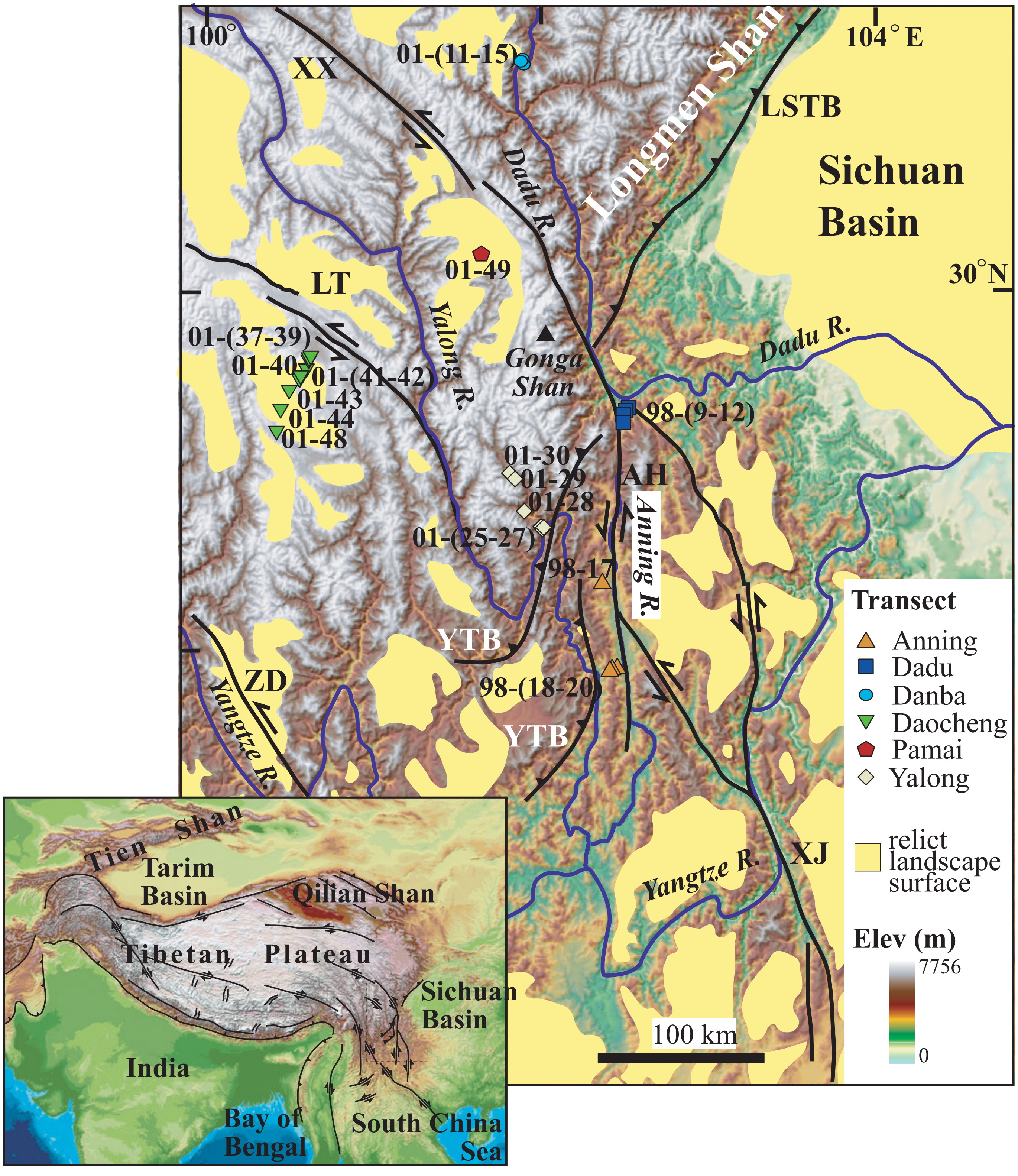

Figure DR1: Sample location map and generalized Cenozoic tectonic structures (from Burchfiel et al., 1995; Wang et al., 1998). Colored symbols represent sample location: shape represents transect and numbers represent individual sample names. Yellow shading outlines extent of relict landscape surface. Note that the Sichuan Basin is not a Cenozoic depocenter. Surface of Sichuan Basin is cut across deformed Mesozoic strata with less than a few hundred meters of Cenozoic sedimentary cover. Abbreviations represent names of major fault structures: LSTB (Longmen Shan Fold and Thrust Belt), XX (Xianshuihe Fault), XJ (Xiaojiang Fault), AH (Anninghe Fault), YTB (Yalong Thrust Belt), LT (Litang Fault, ZD (Zhongdian Fault)